SCIEPublish

Article

Noble Metal Sites Modulated Cyano-COF for Boosted Photocatalytic O_2 to H_2O_2 Production

Yepeng Yang, Binyi Feng, Chengjiao Wang, Chunju Yang, Jingningxi Wu, Yao Yuan and Rao Tao *

Yunnan Key Laboratory of Metal-Organic Molecular Materials and Device, Yunnan Engineering Technology Research Center for Plastic Films, School of Chemistry and Chemical Engineering, Kunming University, Kunming 650214, China; yepengyang@kmu.edu.cn (Y.Y.); 18288371415@163.com (B.F.); 18788066430@163.com (C.W.); 15012381893@163.com (C.Y.); wjnx040701@sina.com (J.W.); 15087989178@163.com (Y.Y.)

* Corresponding author. E-mail: taorao@kmu.edu.cn (R.T.)

Received: 21 June 2025; Accepted: 4 August 2025; Available online: 11 August 2025

ABSTRACT: Photocatalytic O_2 reduction to hydrogen peroxide (H_2O_2) is a promising chemical synthesis pathway with green property. However, the development of efficient and stable photocatalysts that enable high selectivity and activity remains an urgent scientific challenge. Herein, cyano-based covalent organic framework (cyano-COF) photocatalysts modulated by noble metal sites (*i.e.*, Pt, Pd, Au, and Ag), denoted as Pt/cyano-COF, Pd/cyano-COF, Au/cyano-COF, and Ag/cyano-COF, are designed and synthesized. The cyano-group (-C≡N), acting as a strong electron acceptor, interacts with the noble metal sites to establish an efficient electron transfer pathway, which facilitates the separation of photogenerated charges, optimizes the reaction pathway, and thus enables boosted generation of H_2O_2 via the two-step single electron oxygen reduction reaction ($O_2 \rightarrow \cdot O_2^- \rightarrow H_2O_2$). Under visible irradiation, Pt/cyano-COF, Pd/cyano-COF, Au/cyano-COF, and Ag/cyano-COF deliver superior H_2O_2 production rates of 903 ± 24, 1073 ± 35, 963 ± 9, and 851 ± 56 μmol·g^{-1}·h^{-1}, respectively, much higher than that of pristine cyano-COF (577 ± 69 μmol·h^{-1}·g^{-1}). This study offers profound insights into the mechanism of noble metal sites in the solar-driven selective reduction of O_2 to H_2O_2 synthesis.

Keywords: Covalent organic framework; Noble metal; Photocatalysis; Oxygen reduction reaction; Hydrogen peroxide

1. Introduction

Hydrogen peroxide (H_2O_2), a versatile basic chemical and energy carrier, plays a pivotal role in medical disinfection, wastewater treatment, chemical synthesis, rocket fuel, electronic device cleaning, and battery energy storage [1,2]. However, the industrial H_2O_2 production (e.g., anthraquinone method) is characterized by high energy consumption, toxic byproduct formation, and demanding infrastructure requirements [3,4]. Photocatalytic H_2O_2 synthesis from O_2 and H_2O under sunlight represents a promising strategy that integrates renewable energy utilization with the principles of green chemistry [5]. Despite notable advancements, state-of-the-art photocatalysts based on inorganic semiconductors typically exhibit wide bandgaps and high carrier recombination rates [6], while organic polymers are often limited by their relatively slow charge transfer kinetics [7]. In this context, the development of efficient photocatalysts is highly necessary.

Noble metal (e.g., Pd, Pt, Au, *etc.*) nanoparticles (MNPs) are widely recognized for their unique electronic configurations and superior catalytic performance, which confer distinct advantages in photocatalytic H_2O_2 generation. A key contributing factor is the localized surface plasmon resonance (LSPR) effect, which substantially enhances light absorption in the visible to near-infrared wavelength range, thereby expanding the spectral response and promoting the generation of abundant photogenerated carriers [8,9]. Furthermore, their special surface electronic properties and *d*-band characteristics effectively promote charge separation, reduce the activation energy for oxygen reduction, and improve the selectivity toward H_2O_2 photogeneration [10–12]. These metals serve as effective electron mediators, further enhancing the overall catalytic performance. Recent studies have demonstrated that noble metals can modulate the electronic structure of supporting materials, inducing localized electric fields and forming Schottky junctions that

https://doi.org/10.70322/prp.2025.10016

facilitate directional electron transfer, thereby suppressing charge recombination and promoting electron delivery to the surface reduction sites for O_2 [13–15]. Besides, the hyper-dispersion of nano-metals with ultrafine particle sizes reduces the usage of functional material to a minimum while maximizing the exposure of active sites, thereby enhancing both cost-effectiveness and sustainability [16]. Controlled nucleation and growth of confined metal sites, mediated by organic porous functional supports, has been considered as promising to achieve ultrafine, well-dispersed MNPs with optimized catalytic performance [17,18].

Covalent organic frameworks (COFs), an emerging class of crystalline porous polymeric materials, have garnered much attention for their potential in photocatalytic applications [19–21]. COFs possess several advantages for supporting noble metal active sites in photocatalytic applications [22,23]. (i) The robust and highly porous nature of COFs effectively suppresses the aggregation of MNPs. (ii) The interaction between the metal-support interface and COFs significantly modulates the electronic structure of MNPs, offering a novel strategy to regulate catalytic performance and providing a more precise alternative to traditional methods of directly modifying or tuning MNPs. (iii) The well-defined structure of COFs enables precise control over the microenvironment surrounding metal species by grafting specific functional groups onto their channel walls. Despite these benefits, only limited examples have been reported in the literature, with investigations primarily focusing on stabilizing MNPs via electron-donating coordination groups/elements on the COFs [24]. Generally, MNPs are nucleated at specific sites via coordination interactions through electron-donating groups/elements into COFs [25,26], and further controlled through the spatial confinement effect of the ordered channels. In photocatalytic applications, however, the strong coordination interaction might hinder the effective separation of electron-hole pairs.

In this study, noble metals (Pt, Pd, Au, and Ag) modulated cyano-COF photocatalysts with a strong electron-withdrawing group (-C≡N) for efficient H_2O_2 production from O_2 and H_2O are developed. By integrating ultra-highly dispersed Pt, Pd, Au, Ag NPs into cyano-COF, synergistic enhancements in charge separation and surface photocatalytic activity are achieved.

2. Materials and Methods

2.1. Controlled Synthesis of Cyano-COF-Mediated Metal Nanoparticles

According to our reported procedure, cyano-COF was synthesized by a one-step solvent-thermal method [27]. Briefly, 80 mg of trialdehyde, 48 mg of diacetonitrile, and 600 mg of Cs_2CO_3 were added to 2.8 mL of *o*-dichlorobenzene, and degassed 3 times through the freeze-pump-thaw technique and evacuated to an internal pressure of 150 mTorr and flame-sealed. As-synthesized cyano-COF was utilized to mediate the controllable preparation of ultrafine MNPs. A simple suspension impregnation-*in-situ* reduction was performed to prepare cyano-COF supported nano-sized Pt, Pd, Au, and Ag particles. In a typical procedure, 140 mg of cyano-COF powder was added to 20 mL MeOH solution containing 1.9 mg of $PtCl_2$, 2.9 mg of $Pd(OAc)_2$, 2.9 mg of $AgNO_3$, or 2.2 mg of $HAuCl_4$, and stirred at room temperature (r.t., 20~25 °C) for 12 h. These noble metal ions were then reduced by 4.8 mg $NaBH_4$ dissolved in 0.5 mL MeOH, respectively. The obtained powders were filtered, washed with H_2O and MeOH several times, and dried at 65 °C under vacuum overnight. Their metallic contents were determined by inductively coupled plasma (ICP) to be 0.98 wt%, 0.82 wt%, 0.93 wt%, and 0.87 wt%, respectively, which matches well with the theoretical ones (1.00 wt%).

2.2. Photocatalytic H_2O_2 Production

The photocatalyst (2 mg) and 10 mL aqueous solution (H_2O: ethanol = 9:1, by volume) were added into a glass reactor at room temperature. Before illumination, the suspension was ultrasound 20 min, then high-purity oxygen was purged into the solution for 30 min to remain in an O_2-saturated solution and attain adsorption equilibrium. Under the irradiation of an LED lamp ($\lambda > 420$ nm) with an irradiance value of 385 $W \cdot m^{-2}$ (provided by Wuhan Geao Chemical Technology Co., Ltd., Wuhan, China, using bottom-up illumination), 1 mL of suspension was collected at regular intervals, followed by centrifugation. The concentration of H_2O_2 was determined using the *N*, *N*-diethyl-*p*-phenylenediamine peroxidase (DPD-POD) method [28]. Tert-butanol (TBA), *p*-benzoquinone (BQ), and potassium iodate (KIO_3) are employed as scavengers for ·OH, $\cdot O_2^-$, and e^-, respectively. The H_2O_2 photosynthesis under a N_2 or air atmosphere follows the same procedure described above.

3. Results and Discussion

The pristine cyano-functionalized sp^2-carbon conjugated COF (cyano-COF) was synthesized via Knoevenagel condensation between trialdehyde and diacetonitrile under solvothermal conditions. XRD pattern (Figure S1, Supporting Information, SI) confirms that the as-obtained cyano-COF is crystalline, which is in good agreement with that reported in a previous study [29]. Theoretical calculations confirm that cyano-COF exhibits AA overlapping stacking and AB staggered stacking characteristics.

The cyano-COF-mediated Pt/cyano-COF, Pd/cyano-COF, Au/cyano-COF, and Ag/cyano-COF were prepared via a simple suspension impregnation with in-situ $NaBH_4$ reduction (Figure 1a). In contrast to previous studies focusing on the coordination effect of electron-donating groups with MNPs, this work proposes a synergistic interaction between electron-withdrawing groups and MNPs as a mechanism to enhance photogenerated charge separation (Figure 1b). These as-obtained metal/cyano-COF photocatalysts were subsequently characterized by Fourier transform infrared spectroscopy (FT-IR), transmission electron microscopy (TEM), and X-ray photoelectron spectroscopy (XPS). As shown in Figure 1c, the FT-IR spectra of cyano-COF and metal/cyano-COF exhibit a strong C≡N stretching vibration at ~2215 cm^{-1} [29]. Additionally, prominent signal peaks at ~3230 cm^{-1}, corresponding to the C=C stretching vibration [27], are observed. These results confirm that the chemical structure of cyano-COF remains intact following the incorporation of Pt, Pd, Au, and Ag species. TEM images (Figure 1d–k) reveal that these noble MNPs are dispersed on the cyano-COF surface with varying sizes. Specifically, Pt NPs and Pd NPs exhibit uniform diameters of 2.35 ± 1.08 nm and 2.53 ± 0.80 nm, respectively, whereas Au NPs and Ag NPs tend to aggregate into larger particles, with size distributions centered at 3.62 nm and 2.94 nm, respectively. These particle size and distribution differences are primarily attributed to their distinct electronic properties and nucleation-growth kinetics. From the perspective of electronic structure, *d*-orbital electrons of Pt and Pd have high reactivity during bonding. The electron-withdrawing effect of cyano-groups could enhance the electronic interaction between the COFs and Pt (or Pd), which leads to more effective stabilization of the surface atoms of MNPs and a reduction in their surface energy, forming smaller NPs. In contrast, the electronic structures of Au and Ag are relatively stable, with lower *d*-orbital electron reactivity, resulting in weak electronic interactions between these metals and cyano-COF. Consequently, it might be much more challenging to stabilize the surface atoms of Au NPs and Ag NPs, making them more prone to aggregation during the growth process and forming larger particles.

The surface chemical states of these four metal/cyano-COF materials were further characterized using X-ray photoelectron spectroscopy (XPS). As presented in Figure S2 (SI), the XPS survey spectra indicate the presence of C and N elements in both cyano-COF and metal/cyano-COF. The high-resolution C 1s spectra (Figure 2a) of cyano-COF and metal/cyano-COF exhibit two sets of doublets, which are ascribed to C-C/C=C (284.5 eV) and -C≡N (285.7–286.4 eV), corresponding to the carbon elements in the benzene ring and cyano-group, respectively [29]. Compared with pristine cyano-COF (286.4 eV), the C 1s characteristic peak centers of -C≡N in Pt/cyano-COF, Pd/cyano-COF, Au/cyano-COF, and Ag/cyano-COF are reduced by 0.3, 0.1, 0.7, and 0.3 eV, respectively, indicating that the incorporation of noble metals suppresses the electron transfer from carbon to nitrogen. The binding energy of N 1s (~399 eV) shows slight shifts of −0.11, −0.10, 0.02 eV upon the incorporation of Pt, Pd, and Au respectively, indicating the electron-withdrawing nature of the -C≡N group toward Pt NPs and Pd NPs, while a very weak electron-donating property is observed for Au NPs (Figure 2b). The binding energy of N 1s of Ag/cyano-COF was observed to be unchanged. This effect is notably distinct from the previously reported electronic influence of electron-withdrawing anchoring groups on metal species [30].

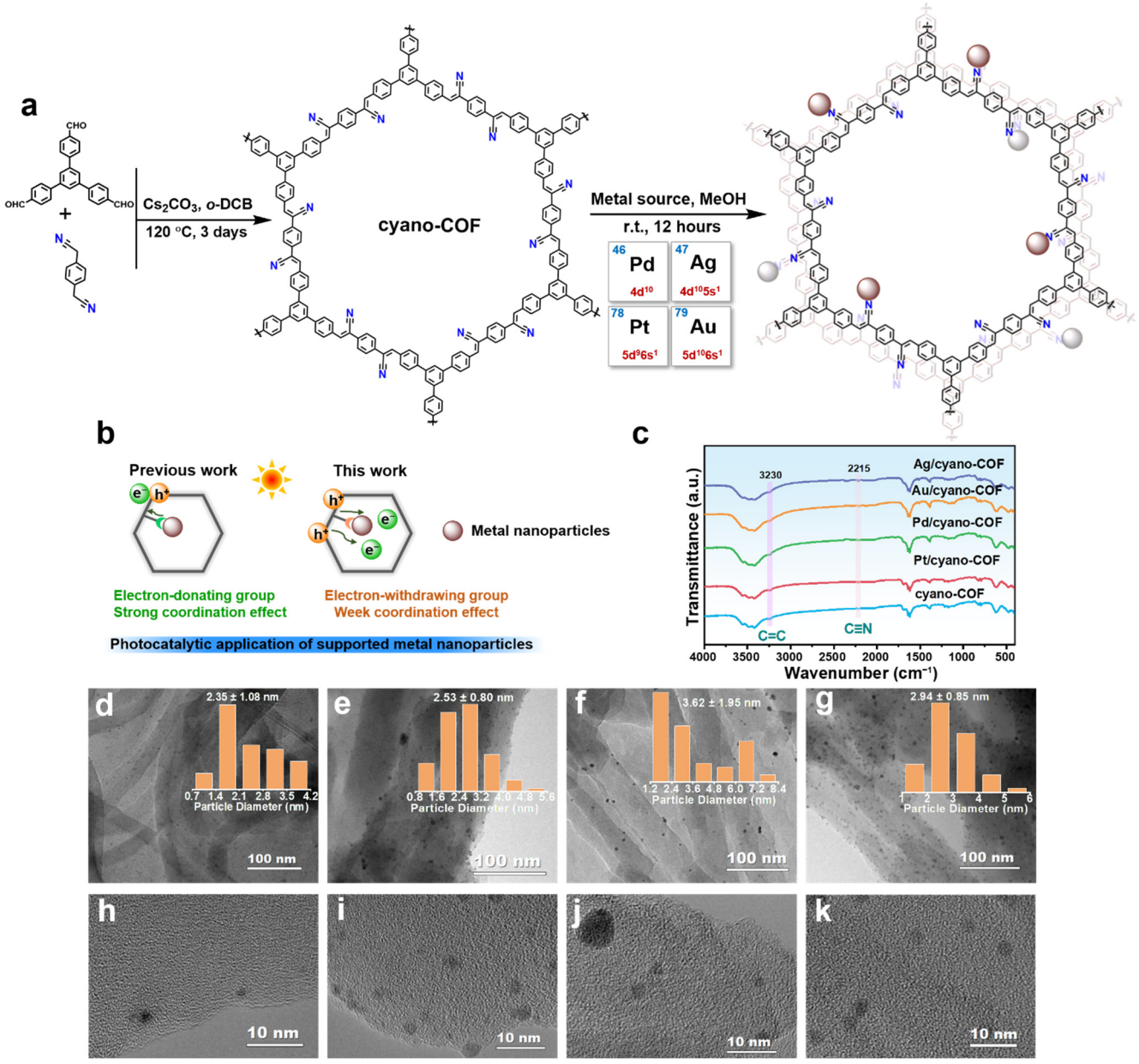

Figure 1. (**a**) Schematic illustration of the preparation process for metal/cyano-COF photocatalysts via suspension impregnation combined with in-situ reduction. (**b**) Proposed ideal of enhancing photogenerated charge separation through the synergistical interaction between electron-withdrawing groups and MNPs. (**c**) FT-IR spectra of cyano-COF and metal/cyano-COF. TEM images and particle size distribution of (**d**,**h**) Pt/cyano-COF, (**e**,**i**) Pd/cyano-COF, (**f**,**j**) Au/cyano-COF, and (**g**,**k**) Ag/cyano-COF.

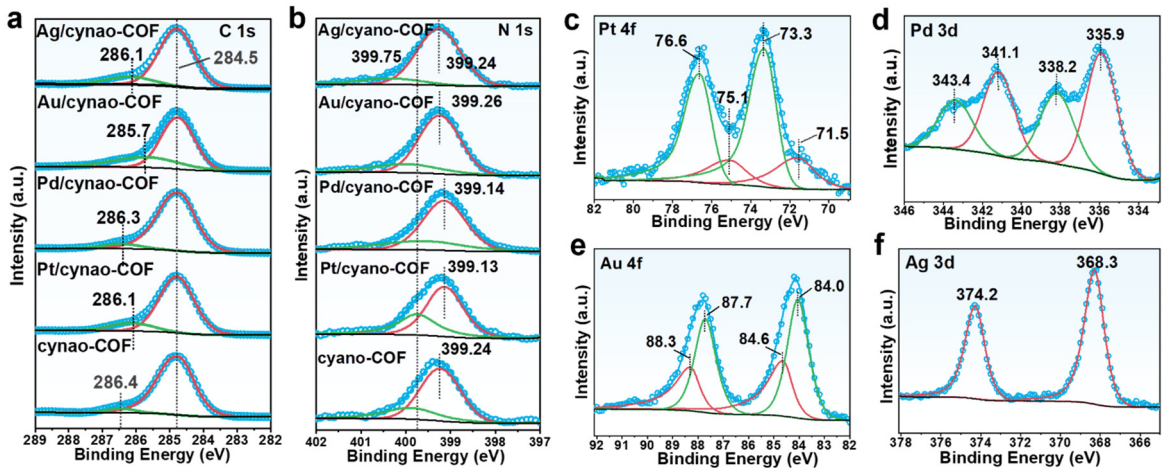

Figure 2. XPS characterization of cyano-COF and metal/cyano-COF: (**a**) C 1s, (**b**) N 1s, (**c**) Pt 4f, (**d**) Pd 3d, (**e**) Au 4f, and (**f**) Ag 3d regions.

The deconvolution analysis of the doublet peaks in the Pt 4f, Pd 3d, and Au 4f regions reveals two distinct sets of doublets. A detailed analysis of the XPS spectra (Figure 2c) confirms the coexistence of two distinct species, Pt(0) and Pt(II), in Pt/cyano-COF. The peaks located at 71.5 eV and 75.1 eV are assigned to the $4f_{7/2}$ and $4f_{5/2}$ spin-orbit components of Pt(0), respectively [31]. Additionally, the higher binding energy peaks at 73.3 eV ($4f_{7/2}$) and 76.6 eV ($4f_{5/2}$) are ascribed to the Pt(II) species, which likely arises from surface oxidation during exposure to air. This phenomenon is commonly observed in supported nano-metal catalysts [32]. The deconvolution of the Pd 3d regions (Figure 2d) reveals two sets of doublets, each comprising a lower-energy band (Pd $3d_{5/2}$) and a higher-energy band (Pd $3d_{3/2}$). The doublet located at 335.9 eV and 341.1 eV is assigned to Pd(0) [33], confirming the successful reduction of Pd(II) to Pd(0). Another set of characteristic peaks at 338.2 eV and 343.4 eV is attributed to PdO [23]. The coexistence of Au(0) and Au(I) species is also observed in Au/cyano-COF (Figure 2e). The peaks centered at 80.0 eV and 87.7 eV are attributed to the $4f_{7/2}$ and $4f_{5/2}$ bands of Au(0), respectively. Additionally, the higher binding energy peaks at 84.6 eV ($4f_{7/2}$) and 88.3 eV ($4f_{5/2}$) are assigned to Au(I) species [34]. The Ag species in Ag/cyano-COF photocatalyst are exclusively present in the chemical states of Ag(0), as indicated by the binding energies of 368.3 eV (Ag $3d_{3/2}$) and 374.2 eV (Ag $3d_{5/2}$) (Figure 2f) [35]. It should be noted here that the binding energy of Ag(0) typically exhibits only a minor variation compared to that of Ag(I). The maximum shift reported in the literature is 0.4 eV for Ag_2O. Such negligible differences in binding energy render the determination of oxidation states particularly challenging, unless XAS measurements are performed [36]. Besides, in almost supported Ag NPs, the XPS region of Ag species is typically found to predominantly exist in the chemical state of Ag(0) [37–39].

Given the sp^2-carbon conjugated framework structure, the electron-withdrawing nature of cyano-groups, and the distinctive electronic structures and properties of these four noble metals (Pt, Pd, Au, and Ag), these metal/cyano-COF materials were then utilized for photocatalytic H_2O_2 synthesis that is a promising and environmentally friendly pathway, offering a viable alternative to traditional energy-intensive technologies. The H_2O_2 photogeneration of metal/cyano-COF was carried out under simulated solar light. As shown in Figure 3a and 3b, Pt/cyano-COF, Pd/cyano-COF, Au/cyano-COF, Ag/cyano-COF exhibit photocatalytic H_2O_2 production rates of 903 ± 24, 1073 ± 35, 963 ± 9, and 851 ± 56 $\mu mol \cdot g^{-1} \cdot h^{-1}$, respectively, representing 1.56, 1.86, 1.67 and 1.47 times higher than that of pristine cyano-COF (577 ± 69 $\mu mol \cdot g^{-1} \cdot h^{-1}$). Furthermore, the cycle durability of these supported metal/cyano-COF photocatalysts was systematically evaluated. As shown in Figure 3c, the production rates of H_2O_2 photosynthesized by the four metal/cyano-COF materials exhibit a slight decrease during the first cycle and remains almost constant in the subsequent three cycles. In the fourth cycle, the H_2O_2 yield of these metal/cyano-COF materials retained more than 66% of initial yields, demonstrating their good stability.

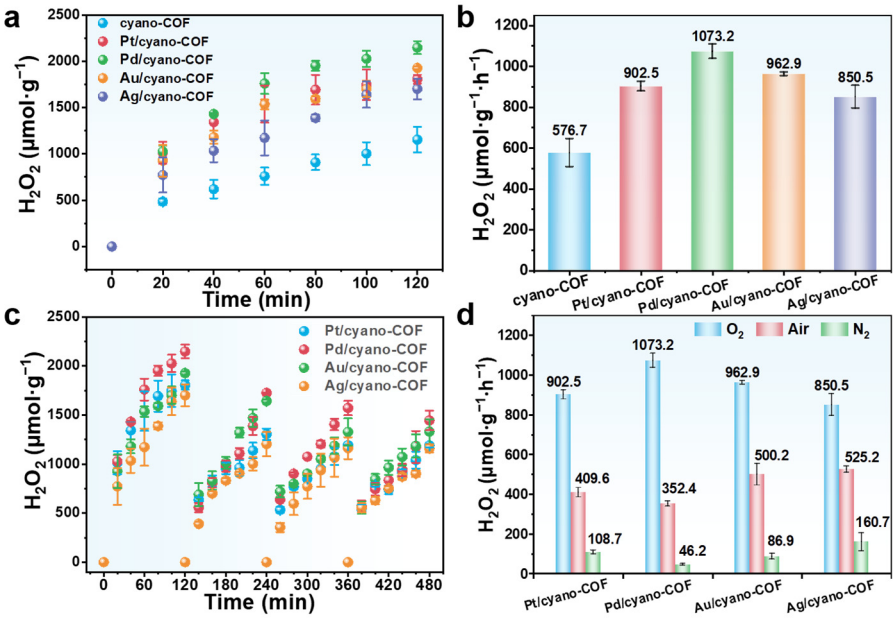

Figure 3. (**a**) Time course of photocatalytic H_2O_2 production for cyano-COF and metal/cyano-COF. (**b**) photocatalytic H_2O_2 production rate over cyano-COF and metal/cyano-COF. (**c**) cycling durability of H_2O_2 production over metal/cyano-COF. (**d**) photocatalytic production of H_2O_2 over metal/cyano-COF under different atmosphere conditions.

To gain deep insights into the enhanced photocatalytic performance of H_2O_2 photogeneration, controlled experiments were conducted under different atmospheres (O_2, air, and N_2). As shown in Figure 3d, Pt/cyano-COF, Pd/cyano-COF, Au/cyano-COF, and Ag/cyano-COF exhibit much higher H_2O_2 production rates in an O_2 atmosphere compared to those in air and N_2. Specifically, under air condition, the H_2O_2 photosynthesis yields for Pt/cyano-COF, Pd/cyano-COF, Au/cyano-COF, and Ag/cyano-COF are 410 ± 24, 353 ± 13, 500 ± 54, and 525 ± 16 $\mu mol \cdot g^{-1} \cdot h^{-1}$, respectively. In contrast, under a N_2-saturated atmosphere, the corresponding yields are significantly lower, with yields of 109 ± 10, 46 ± 4, 87 ± 15, and 161 ± 46 $\mu mol \cdot g^{-1} \cdot h^{-1}$, respectively. These results indicate that O_2 is the key raw material for photocatalytic synthesis of H_2O_2 over these four metal/cyano-COF materials.

To understand the photocatalytic mechanism of H_2O_2 synthesis, the light absorption properties of cyano-COF and metal/cyano-COF were studied using ultraviolet-visible diffuse reflectance spectroscopy (UV-Vis DRS). As shown in Figure 4a, all materials exhibit strong absorption across UV and visible regions. Based on Tauc plots, the optical band gaps of cyano-COF, Pt/cyano-COF, Pd/cyano-COF, Au/cyano-COF, and Ag/cyano-COF are determined to be 2.37, 2.39, 2.37, 2.38, and 2.36 eV, respectively (Figure S3, SI).

Mott-Schottky (M-S) test (Figure S4, SI) was employed to determine the electronic band positions of these photocatalysts. The positive slopes of the M-S curves indicate that both cyano-COF and metal/cyano-COF are n-type semiconductors [40]. The corresponding flat band potentials of cyano-COF, Pt/cyano-COF, Pd/cyano-COF, Au/cyano-COF, and Ag/cyano-COF are −0.84, −0.83, −0.84, −0.74, and −0.73 V *vs.* Ag/AgCl, respectively. Given that the flat band potential of n-type semiconductors is typically more positive (by 0.1–0.3 V) than the conduction band (CB) potentials [41], the lowest unoccupied molecular orbital (LUMO) positions of cyano-COF, Pt/cyano-COF, Pd/cyano-COF, Au/cyano-COF, and Ag/cyano-COF are estimated to be −0.74, −0.73, −0.74, −0.64, and −0.63 V *vs.* NHE, respectively. Based on the band edges derived from Tauc plots, the relative positions of the LUMO and the highest occupied molecular orbital (HOMO) for cyano-COF and metal/cyano-COF are illustrated in Figure 4b. Since the LUMO of all materials is more negative than the potentials for both the concerted $1e^-$ oxygen reduction reaction (ORR) ($O_2/\cdot O_2^-$, −0.33 V *vs.* NHE) and the $2e^-$ ORR (O_2/H_2O_2, 0.68 V *vs.* NHE), which indicates that all materials are favorable for the photoreduction of O_2 to produce $\cdot O_2^-$, followed by the formation of H_2O_2 [42,43].

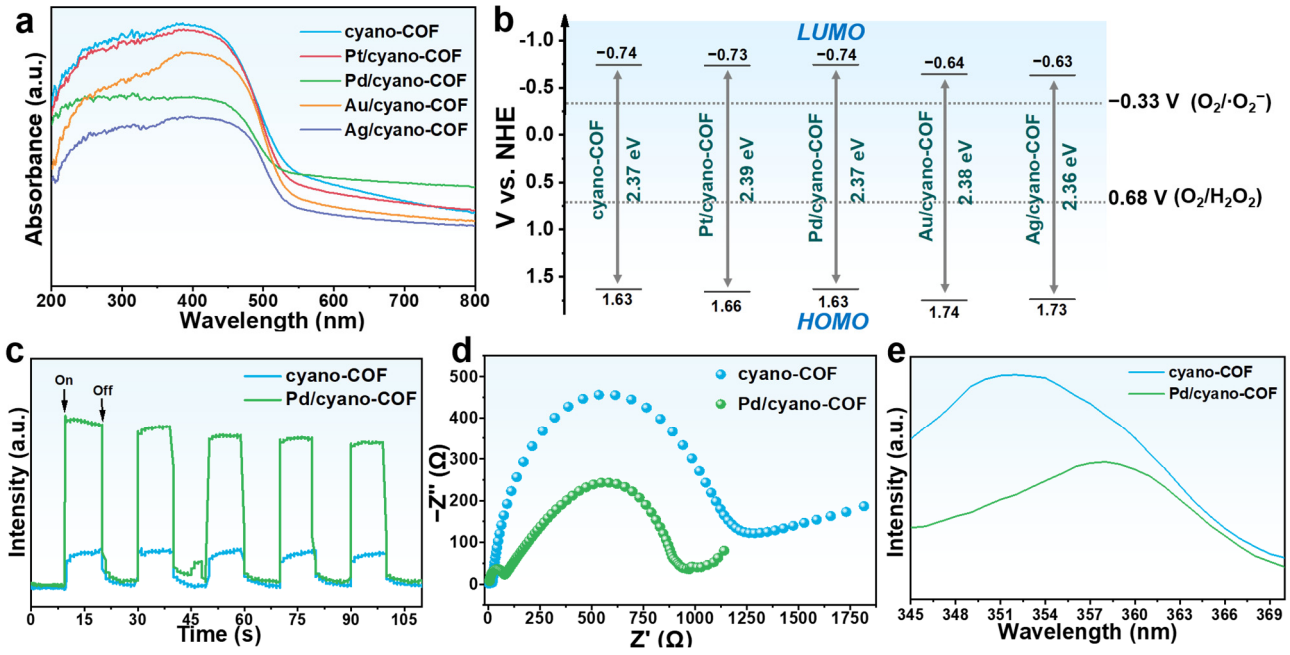

Figure 4. (**a**) UV-vis DRS spectra and (**b**) energy band structure of cyano-COF and metal/cyano-COF. (**c**) transient photocurrent response, (**d**) Nyquist plots and (**e**) PL spectra of cyano-COF and Pd/cyano-COF.

Given the analogous optical properties of the four noble metals supported on cyano-COF and their performance in photocatalytic H_2O_2 synthesis, cyano-COF and Pd/cyano-COF were utilized as discussed subjects for subsequent experiments to further investigate the photocatalytic mechanism. The photocurrent responses of cyano-COF and Pd/cyano-COF are presented in Figure 4c. Pd/cyano-COF has a significantly stronger photocurrent response compared to pristine cyano-COF, indicating efficient photoinduced charge transfer between cyano-COF and Pd NPs. The Nyquist plots (Figure 4d) corroborate this observation. The smaller semicircle diameter in the high-frequency region for

Pd/cyano-COF, relative to that of cyano-COF, reflects a reduced charge transfer impedance, thereby enhancing charge separation and transfer efficiency, which promotes the participation of more e^- and h^+ during the photocatalytic H_2O_2 formation [44]. In addition, the substantial reduction in photoluminescence (PL) emission intensity (Figures 4e and S5 (SI)) confirms the effective suppression of charge carrier recombination in Pd-modified cyano-COF. The enhanced charge separation is attributed to the synergistic interaction between noble MNPs and cyano-COF.

Photocatalytic H_2O_2 production exhibits significant potential but encounters developmental challenges, primarily the rapid recombination of photogenerated charge carriers (e^- and h^+) and the inefficiency of the water oxidation reaction in pure water systems. The application of sacrificial electron donors, such as methanol, EtOH, isopropanol, and benzyl alcohol, addresses these issues by undergoing oxidation more readily than water. This facilitates the effective consumption of photogenerated h^+, suppresses charge recombination, and substantially enhances H_2O_2 yield. Organic photocatalysts benefit particularly from this approach, as efficient h^+ scavenging prevents self-oxidation and improves long-term stability [45,46]. Compared with the pure water system, the introduction of EtOH consumes photogenerated h^+ and facilitates the separation of e^--h^+ pairs, thereby enhancing the catalytic performance. As exhibited in Figure 5a, cyano-COF and metal/cyano-COF have 1.40–2.17 times higher H_2O_2 yields in the presence of EtOH as a sacrificial agent of h^+ compared to the pure water system. Control experiments were carried out to scavenge other active intermediates to elucidate the photocatalytic mechanism of H_2O_2 synthesis over cyano-COF and metal/cyano-COF. TBA, BQ, and KIO_3 are commonly utilized as scavengers for ·OH, $\cdot O_2^-$, and e^-, respectively [47,48]. The addition of TBA exerts no significant influence on the H_2O_2 yield, suggesting that ·OH is not the predominant active species in the photocatalytic reaction. The presence of KIO_3 resulted in a reduced rate of photocatalytic H_2O_2 production, which is attributed to its scavenging effect on photogenerated e^-. Furthermore, KIO_3 is employed as an e^- capture agent to suppress H_2O_2 production under N_2 atmosphere, indicating that ORR plays a dominant role in this process [49]. Atmosphere experiments demonstrated that ORR is the primary pathway for photocatalytic H_2O_2 production over metal/cyano-COF (Figure 3d). The pronounced inhibitory effect of BQ on H_2O_2 production strongly suggests that$\cdot O_2^-$ serves as a critical intermediate in the formation mechanism of H_2O_2 on metal/cyano-COF. Furthermore, electron paramagnetic resonance (EPR) spectroscopy by 5,5-dimethyl-1-pyrroline *N*-oxide (DMPO) was employed to identify the presence of $\cdot O_2^-$ during the photocatalytic process [16,50]. As depicted in Figure 5b, a characteristic EPR signal of DMPO-$\cdot O_2^-$ signals was detected for Pd/cyano-COF under illumination, whereas no such signals were observed in the dark. This result is consistent with the results of the above sacrificial agent experiments. Consequently, it can be concluded that the photocatalytic production of H_2O_2 proceeds via a sequential two-step $1e^-$-ORR process (Figure 5c) ($O_2 \rightarrow \cdot O_2^- \rightarrow H_2O_2$) [42]. During the photocatalytic process, photogenerated electrons are transferred from the conduction band of cyano-COF to the noble metals, forming a highly active electron-enriched region. These electrons can subsequently react with oxygen molecules adsorbed on the noble metal surface to generate $\cdot O_2^-$, which further participates in reactions leading to the efficient formation of H_2O_2 [51–53].

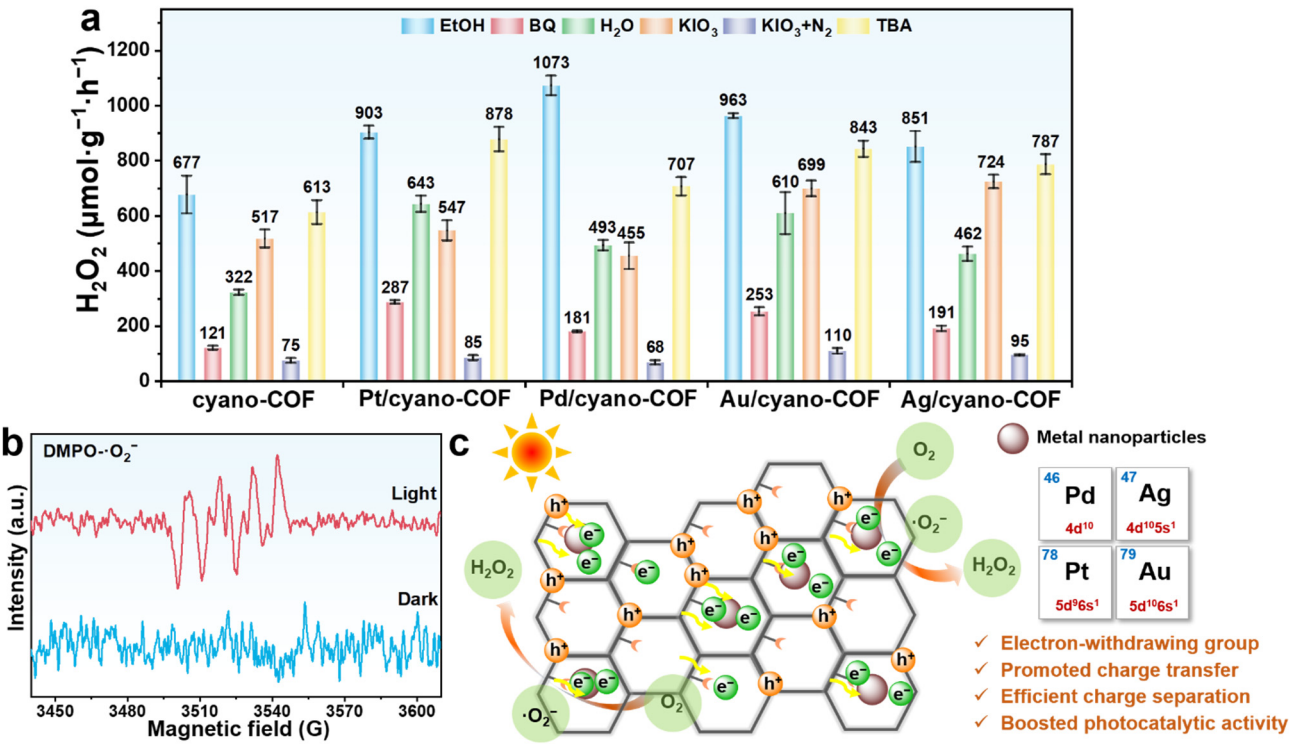

Figure 5. (**a**) Photocatalytic H_2O_2 production rates of cyano-COF and metal/cyano-COF in the presence of various sacrificial agents. (**b**) EPR spectra in the presence of DMPO under visible-light illumination. (**c**) Schematic illustration of the proposed catalytic mechanism for photocatalytic H_2O_2 production over metal/cyano-COF.

4. Conclusions

In summary, four noble metal-modulated cyano-COF photocatalysts, including Pt/cyano-COF, Pd/cyano-COF, Au/cyano-COF, and Ag/cyano-COF, were successfully synthesized through a straightforward suspension impregnation with in-situ $NaBH_4$ reduction. Efficient charge transfer between the noble MNPs and the cyano-COF support enables enhanced photocatalytic O_2 reduction to H_2O_2 ($O_2 \rightarrow \cdot O_2^- \rightarrow H_2O_2$). Among these catalysts, Pd/cyano-COF exhibits both optimal adsorption capacity and superior electron transfer ability, which collectively contribute to its excellent surface catalytic performance, achieving the highest H_2O_2 production rate of 1073 ± 35 μmol·g^{-1}·h^{-1}. This study proposes a feasible design strategy that the electron-withdrawing group and the noble MNPs synergistically promote the efficient separation of photogenerated carriers.

Supplementary Materials

The following supporting information can be found at: https://www.sciepublish.com/article/pii/632, Figure S1: XRD pattern of cyano-COF; Figure S2: Wide scan XPS spectra of cyano-COF and metal/cyano-COF; Figure S3: Tauc plots of cyano-COF and metal/cyano-COF; Figure S4: Mott-Schottky curves of cyano-COF and metal/cyano-COF; Figure S5: Photoluminescence spectra of cyano-COF and metal/cyano-COF.

Author Contributions

Y.Y. (Yepeng Yang): Methodology, Validation, Investigation, Writing-review & editing. B.F.: Methodology, Validation, Investigation. C.W.: Investigation. C.Y.: Investigation. J.W.: Validation. Y.Y. (Yao Yuan): Validation. R.T.: Writing-review & editing, Supervision, Funding acquisition, Conceptualization.

Ethics Statement

Not applicable.

Informed Consent Statement

Not applicable.

Data Availability Statement

Data will be made available on request.

Funding

This work was supported by Yunnan Fundamental Research Project (202401AU070013), Cooperative Research Program of Yunnan Provincial Undergraduate Universities' Association (Grant 202401BA070001-117, 202301BA070001-128), Talent Introduction Project of Kunming University (Grant YJL23018), Yunnan Key Laboratory of Metal-Organic Molecular Materials and Device Independent Research Projects (Grant YNMO-ZD-2405, YNMO-ZD-2407), Education Department Project of Yunnan Province (Grant 2025Y1068, 2025Y1073, 2025Y1059), College Students' Innovative Entrepreneurial Training Plan Program (202411393002, 202411393008), and the Frontier Research Team of Kunming University 2023.

Declaration of Competing Interest

The authors declare that they have no known competing financial interests or personal relationships that could have appeared to influence the work reported in this paper.

References

1. Zhang P, Tong Y, Liu Y, Vequizo JJM, Sun H, Yang C, et al. Heteroatom dopants promote two-electron O_2 reduction for photocatalytic production of H_2O_2 on polymeric carbon nitride. *Angew. Chem. Int. Edit.* **2020**, *59*, 16209–16217. doi:10.1002/anie.202006747.
2. Tan D, Zhuang R, Chen R, Ban M, Feng W, Xu F, et al. Covalent organic frameworks enable sustainable solar to hydrogen peroxide. *Adv. Funct. Mater.* **2023**, *34*, 2311655. doi:10.1002/adfm.202311655.
3. Hou H, Zeng X, Zhang X. Production of hydrogen peroxide by photocatalytic processes. *Angew. Chem. Int. Ed.* **2020**, *59*, 17356–17376. doi:10.1002/anie.201911609.
4. Campos-Martin JM, Blanco-Brieva G, Fierro JL. Hydrogen peroxide synthesis: An outlook beyond the anthraquinone process. *Angew. Chem. Int. Ed.* **2006**, *45*, 6962–6984.
5. Yang Y, Wang C, Li Y, Liu K, Ju H, Wang J, et al. Porous organic framework materials for photocatalytic H_2O_2 production. *J. Mater. Sci. Technol.* **2024**, *200*, 185–214. doi:10.1016/j.jmst.2024.02.062.
6. Liu T, Pan Z, Vequizo JJM, Kato K, Wu B, Yamakata A, et al. Overall photosynthesis of H_2O_2 by an inorganic semiconductor. *Nat. Commun.* **2022**, *13*, 1034. doi:10.1038/s41467-022-28686-x.
7. Yu X, Hu Y, Shao C, Huang W, Li Y. Polymer semiconductors: A unique platform for photocatalytic hydrogen peroxide production. *Mater. Today* **2023**, *71*, 152–173. doi:10.1016/j.mattod.2023.10.005.
8. Sheng H, Wang J, Huang J, Li Z, Ren G, Zhang L, et al. Strong synergy between gold nanoparticles and cobalt porphyrin induces highly efficient photocatalytic hydrogen evolution. *Nat. Commun.* **2023**, *14*, 1528. doi:10.1038/s41467-023-37271-9.
9. Liu Y, Huang S, Huang X, Ma D. Enhanced photocatalysis of metal/covalent organic frameworks by plasmonic nanoparticles and homo/hetero-junctions. *Mater. Horiz.* **2024**, *11*, 1611–1637. doi:10.1039/d3mh01645e.
10. Shi H, Ding S, Tian Y, Li S, Ye L, Li R, et al. Weakened interfacial O_2 adsorption by modulating charge density of Pd atom in the vertical-growth Bi nanosheets toward boosted H_2O_2 photosynthesis. *J. Energy Chem.* **2025**, *107*, 682–692. doi:10.1016/j.jechem.2025.03.083.
11. Xue Q, Wang Z, Han S, Liu Y, Dou X, Li Y, et al. Ligand engineering of Au nanoclusters with multifunctional metalloporphyrins for photocatalytic H_2O_2 production. *J. Mater. Chem. A* **2022**, *10*, 8371–8377. doi:10.1039/d2ta00720g.
12. Fang M, Tan X, Liu Z, Hu B, Wang X. Recent progress on metal-enhanced photocatalysis: A review on the mechanism. *Research* **2021**, *2021*, 9794329. doi:10.34133/2021/9794329.
13. Song M, Shao H, Chen Y, Deng X, Chen Y, Yao Y, et al. Visible light-driven H_2O_2 synthesis over Au/C_3N_4: Medium-sized Au nanoparticles exhibiting suitable built-in electric fields and inhibiting reverse H_2O_2 decomposition. *Phys. Chem. Chem. Phys.* **2022**, *24*, 29557–29569. doi:10.1039/d2cp04202a.
14. Sun Z-X, Sun K, Gao M-L, Metin Ö, Jiang H-L. Optimizing Pt electronic states through formation of a schottky junction on non-reducible metal-organic frameworks for enhanced photocatalysis. *Angew. Chem. Int. Ed.* **2022**, *61*, e202206108. doi:10.1002/anie.202206108.
15. Chen J, Su Y, Wang Y, Wei Z, Zheng Z, Yuan H, et al. Ultrahigh loading of confined plasmonic nanoparticles within thiol-functionalized metal-organic frameworks for efficient photocatalytic CO_2 reduction to CO and hydrocarbons. *Nano Res.* **2025**, *18*, 94907181. doi:10.26599/nr.2025.94907181.
16. Liu Y, Li L, Tan H, Ye N, Gu Y, Zhao S, et al. Fluorination of covalent organic framework reinforcing the confinement of Pd nanoclusters enhances hydrogen peroxide photosynthesis. *J. Am. Chem. Soc.* **2023**, *145*, 19877–19884.

doi:10.1021/jacs.3c05914.
17. Tao R, Yang T, Li X, Gao H, Liu S, Wang Y, et al. $SbPh_3$-based organic molecular cage for size-controlled preparation and stabilization of palladium nanoparticles. *Appl. Surf. Sci.* **2023**, *640*, 158332. doi:10.1016/j.apsusc.2023.158322.
18. Tao R, Zheng Y, Wang Y, Yang T, Qiu L. Highly dispersed Pd nanoclusters supported on covalent triazine-based frameworks for highly efficient aryl nitro reduction and Ullmann coupling. *Micropor. Mesopor. Mat.* **2023**, *362*, 112796. doi:10.1016/j.micromeso.2023.112796.
19. Zhao W, Yan P, Li B, Bahri M, Liu L, Zhou X, et al. Accelerated synthesis and discovery of covalent organic framework photocatalysts for hydrogen peroxide production. *J. Am. Chem. Soc.* **2022**, *144*, 9902–9909. doi:10.1021/jacs.2c02666.
20. Wei S, Hou R, Zhu Q, Shakir I, Fang Z, Duan X, et al. Hybrid materials based on covalent organic frameworks for photocatalysis. *InfoMat* **2024**, *7*, e12646. doi:10.1002/inf2.12646.
21. Yang Y, Li Y, Ma X, Xie L, Lv D, Jiang L, et al. Direct Z-scheme WO_3/covalent organic framework (COF) heterostructure for enhanced photocatalytic hydrogen peroxide production in water. *Catal. Sci. Technol.* **2023**, *13*, 5599–5609. doi:10.1039/d3cy00878a.
22. Tao R, Ma X, Wei X, Jin Y, Qiu L, Zhang W. Porous organic polymer material supported palladium nanoparticles. *J. Mater. Chem. A* **2020**, *8*, 17360–17391. doi:10.1039/d0ta05175f.
23. Tao R, Shen X, Hu Y, Kang K, Zheng Y, Luo S, et al. Phosphine-based covalent organic framework for the controlled synthesis of broad-scope ultrafine nanoparticles. *Small* **2020**, *16*, 1906005. doi:10.1002/smll.201906005.
24. Guo M, Guan X, Meng Q, Gao ML, Li Q, Jiang HL. Tailoring catalysis of encapsulated platinum nanoparticles by pore wall engineering of covalent organic frameworks. *Angew. Chem. Int. Ed.* **2024**, *63*, e202410097. doi:10.1002/anie.202410097.
25. Xu F, Liang B, Liu L, Hu X, Weng B. Pd nanoparticle-decorated covalent organic frameworks for enhanced photocatalytic tetracycline hydrochloride degradation and hydrogen evolution. *Chem. Commun.* **2023**, *59*, 6387–6390. doi:10.1039/d3cc01425h.
26. Chen L, Chen G, Gong C, Zhang Y, Xing Z, Li J, et al. Low-valence platinum single atoms in sulfur-containing covalent organic frameworks for photocatalytic hydrogen evolution. *Nat. Commun.* **2024**, *15*, 10501. doi:10.1038/s41467-024-54959-8.
27. Tao R, Feng B, Wang C, Zhang H, Chen R, Liu K, et al. Feasible preparation of preferentially oriented (111) Pd nanocrystals supported on cyano-COFs for ultrahigh activity in C-C cross-couplings. *J. Catal.* **2024**, *432*. doi:10.1016/j.jcat.2024.115399.
28. Yang Y, Wang C, Hu Z, Zhang X, Wu J, You F, et al. Accelerated sonochemical fabrication of MIn_2S_4 (M = Zn, Mg, Ni, Co) for ultrahigh photocatalytic hydrogen peroxide production. *Ultrason. Sonochem.* **2024**, *106*, 106903. doi:10.1016/j.ultsonch.2024.106903.
29. Zhuang X, Zhao W, Zhang F, Cao Y, Liu F, Bi S, et al. A two-dimensional conjugated polymer framework with fully sp^2-bonded carbon skeleton. *Polym. Chem.* **2016**, *7*, 4176–4181. doi:10.1039/c6py00561f.
30. Li S, Zhou C, Hu J, Duan A, Xu C, Wang X. PdIr nanoparticles on NH_2-functionalized dendritic mesoporous silica nanospheres for efficient dehydrogenation of formic acid. *J. Catal.* **2023**, *426*, 153–161. doi:10.1016/j.jcat.2023.07.014.
31. Wu J, Xi X, Zhu W, Yang Z, An P, Wang Y, et al. Boosting photocatalytic hydrogen evolution via regulating Pt chemical states. *Chem. Eng. J.* **2022**, *442*, 136334. doi:10.1016/j.cej.2022.136334.
32. Lu S, Hu Y, Wan S, McCaffrey R, Jin Y, Gu H, et al. Synthesis of ultrafine and highly dispersed metal nanoparticles confined in a thioether-containing covalent organic framework and their catalytic applications. *J. Am. Chem. Soc.* **2017**, *139*, 17082–17088. doi:10.1021/jacs.7b07918.
33. Tao R, Kang K, Li X, Li R, Huang R, Jin Y, et al. Controlled synthesis of palladium nanoparticles with size-dependent catalytic activities enabled by organic molecular cages. *Inorg. Chem.* **2021**, *60*, 12517–12525. doi:10.1021/acs.inorgchem.1c01723.
34. Zhong W, Meng A, Su Y, Yu H, Han P, Yu J. Achieving free-electron transfer reversal and dz^2-orbital occupancy modulation on core-shell NiS@Au cocatalysts for highly selective H_2O_2 photosynthesis. *Angew. Chem. Int. Ed.* **2025**, *64*, e202425038. doi:10.1002/anie.202425038.
35. Yang Y, Li Y, Lu Y, Chen Z, Luo R. A three-dimensional azo-bridged porous porphyrin framework supported silver nanoparticles as the state-of-the-art catalyst for the carboxylative cyclization of propargylic alcohols with CO_2 under ambient conditions. *ACS Catal.* **2024**, *14*, 10344–10354. doi:10.1021/acscatal.4c02391.
36. Kaushik VK. XPS core level spectra and Auger parameters for some silver compounds. *J. Electron. Spectrosc. Relat. Phenom.* **1991**, *56*, 273–277. doi:10.1016/0368-2048(91)85008-H.
37. Zeng G, Li G, Yuan W, Liu J, Wu Y, Li M, et al. Ag nanoparticle-mediated LSPR effect and electron transfer for enhanced oxidative degradation process of g-C_3N_5 nanoflowers. *Sep. Purif. Technol.* **2025**, *353*, 128484. doi:10.1016/j.seppur.2024.128484.
38. Lai W, Jiao Y, Liu Y, Fang W, Wang Z, Guiver MD, et al. Engineering ultra-small Ag nanoparticles with enhanced activity in microporous polymer membranes for C_2H_4/C_2H_6 Separation. *Adv. Mater.* **2025**, *37*, 2416851. doi:10.1002/adma.202416851.
39. Liu Q, Bi H, Zhao R, Yang X, Chen F, Shen Z. Fully exposed silver clusters enabling highly efficient photocatalytic H_2O_2 production in pure water. *Angew. Chem. Int. Ed.* **2025**, e202511687 doi:10.1002/anie.202511687.
40. Li S, Yu H, Wang Y, Wang S, Zhang L, Zhu P, et al. Engineering covalently integrated COF@CeO_2 Z-scheme heterostructure

for visible light driven photocatalytic CO_2 conversion. *Appl. Surf. Sci.* **2023**, *615*, 156335. doi:10.1016/j.apsusc.2023.156335.

41. Liu S, Jiang X, Waterhouse GIN, Zhang Z-M, Yu L-M. Construction of Z-scheme Titanium-MOF/plasmonic silver nanoparticle/NiFe layered double hydroxide photocatalysts with enhanced dye and antibiotic degradation activity under visible light. *Sep. Purif. Technol.* **2021**, *278*, 119525. doi:10.1016/j.seppur.2021.119525.
42. Yang Y, Kang J, Li Y, Liang J, Liang J, Jiang L, et al. Enhanced photocatalytic hydrogen peroxide production activity of imine-linked covalent organic frameworks via modification with functional groups. *New J. Chem.* **2022**, *46*, 21605–21614. doi:10.1039/d2nj03744k.
43. Chen Z, Yao D, Chu C, Mao S. Photocatalytic H_2O_2 production systems: Design strategies and environmental applications. *Chem. Eng. J.* **2023**, *451*, 138489. doi:10.1016/j.cej.2022.138489.
44. Bao T, Xi Y, Zhang C, Du P, Xiang Y, Li J, et al. Highly efficient nitrogen fixation over S-scheme heterojunction photocatalysts with enhanced active hydrogen supply. *Natl. Sci. Rev.* **2024**, *11*, nwae093. doi:10.1093/nsr/nwae093.
45. Xin J, Shao J, Yu X, Huang W, Li Y. Deciphering the controversial role of sacrificial agents in photocatalytic H_2O_2 production: Promoters or source of artifacts? *ACS Energy Lett.* **2025**, *10*, 3485–3491. doi:10.1021/acsenergylett.5c01771.
46. Xu S, Chen K, Cai Y, Ren S, Chu W, Song M, et al. Unveiling the neglected role of alcohols and phenolic compounds in photocatalysis H_2O_2 generation chemistry. *Water Res.* **2025**, *285*, 124139. doi:10.1016/j.watres.2025.124139.
47. Zhang Y, Qiu J, Zhu B, Fedin MV, Cheng B, Yu J, et al. ZnO/COF S-scheme heterojunction for improved photocatalytic H_2O_2 production performance. *Chem. Eng. J* **2022**, *444*, 136584. doi:10.1016/j.cej.2022.136584.
48. Jin Z, Jin S, Tang X, Tan W, Wang D, Song S, et al. Rational design of conjugated acetylenic Polymers enables a two-electron water oxidation pathway for enhanced photosynthetic hydrogen peroxide generation. *Small* **2023**, *20*, 2305004. doi:10.1002/smll.202305004.
49. Yao Y, Zhu C, Liu R, Fang Q, Song S, Chen B, et al. Synergistic tri-efficiency enhancement utilizing functionalized covalent organic frameworks for photocatalytic H_2O_2 production. *Small* **2024**, *20*, 2404885. doi:10.1002/smll.202404885.
50. Xu H, Wang Y, Xu Y, Wang Q, Zhuang M, Liao Q, et al. Integrating multipolar structures and carboxyl groups in sp^2-carbon conjugated covalent organic frameworks for overall photocatalytic hydrogen peroxide production. *Angew. Chem. Int. Ed.* **2024**, *136*, e202408802. doi:10.1002/anie.202408802.
51. Zhu Q, Xu Z, Qiu B, Xing M, Zhang J. Emerging cocatalysts on g-C_3N_4 for photocatalytic hydrogen evolution. *Small* **2021**, *17*, 2101070. doi:10.1002/smll.202101070.
52. Yin X, Gao D, Xu J, Zhao B, Wang X, Yu J, et al. Platinum-induced nanolization and electron-deficient gold in platinum@gold cocatalyst for efficient photocatalytic hydrogen peroxide production. *J. Colloid Interface Sci.* **2025**, *678*, 1249–1258. doi:10.1016/j.jcis.2024.09.195.
53. Wang G, Huang T, Tan Y, Liu S, Wu R, Fang Z, et al. Effect of photodeposited noble metal nanoparticles on the sacrificial-agent-free H_2O_2 photosynthesis performance of g-C_3N_4. *ACS Appl. Nano Mater.* **2025**, *8*, 6125–6132. doi:10.1021/acsanm.5c00311.